

REPORT DOCUMENTATION PAGE				Form Approved OMB No. 0704-0188	
Public reporting burden for this collection of information is estimated to average 1 hour per response, including the time for reviewing instructions, searching existing data sources, gathering and maintaining the data needed, and completing and reviewing this collection of information. Send comments regarding this burden estimate or any other aspect of this collection of information, including suggestions for reducing this burden to Department of Defense, Washington Headquarters Services, Directorate for Information Operations and Reports (0704-0188), 1215 Jefferson Davis Highway, Suite 1204, Arlington, VA 22202-4302. Respondents should be aware that notwithstanding any other provision of law, no person shall be subject to any penalty for failing to comply with a collection of information if it does not display a currently valid OMB control number. PLEASE DO NOT RETURN YOUR FORM TO THE ABOVE ADDRESS.					
1. REPORT DATE (DD-MM-YYYY) 09-09-2003		2. REPORT TYPE Article in Conference Proceeding		3. DATES COVERED (From - To) 1 Jan 2003 – 31 Jul 2003	
4. TITLE AND SUBTITLE Object Characterization from Spectral Data				5a. CONTRACT NUMBER F29601-00-D-0204	
				5b. GRANT NUMBER N/A	
				5c. PROGRAM ELEMENT NUMBER 63444F	
6. AUTHOR(S) K. Luu, C. Matson, M. Giffin, K. Hamada, J. Lambert, and J. Snodgrass				5d. PROJECT NUMBER 4868/4983	
				5e. TASK NUMBER B3	
				5f. WORK UNIT NUMBER BH	
7. PERFORMING ORGANIZATION NAME(S) AND ADDRESS(ES) AFRL/DEBI (Det 15) 535 Lipoa Parkway Ste 200 Kihei HI 96753				8. PERFORMING ORGANIZATION REPORT NUMBER AFRL/DE 23-420	
9. SPONSORING / MONITORING AGENCY NAME(S) AND ADDRESS(ES) AFRL/DEBI (Det 15) 3550 Aberdeen SE Kirtland AFB NM 87117-5776				10. SPONSOR/MONITOR'S ACRONYM(S)	
				11. SPONSOR/MONITOR'S REPORT NUMBER(S)	
12. DISTRIBUTION / AVAILABILITY STATEMENT Approved for public release; distribution is unlimited.					
13. SUPPLEMENTARY NOTES K. Luu, C. Matson, M. Giffin, K. Hamada, J. Lambert, and J. Snodgrass, "Object Characterization from Spectral Data," 2003 AMOS Technical Conference, Maui, Hawaii, 8-13 September 2003.					
14. ABSTRACT In general, the task of identifying the shape, function, and status of objects from nonimaging temporally-resolved spectral data is impossible. This is due to the limited degrees of freedom in the data as compared to the degrees of freedom that define shape, function, and status. However, by modeling objects as combinations of simple shapes with simple reflective and spectral characteristics, the problem though daunting is expected to become tractable due to the reduction of degrees of freedom in object space. One anticipated result from this modeling process is that the properties of null and near-null object features can be characterized; that is, an object can be characterized as a set of observable features summed with null or near-null features that perturb the measurement only slightly or not at all. The initial development of classes presented in this paper is a first step towards an inversion procedure to map spectral data into classes.					
15. SUBJECT TERMS Satellites, color photometry data					
16. SECURITY CLASSIFICATION OF:			17. LIMITATION OF ABSTRACT UNLIMITED	18. NUMBER OF PAGES 12	19a. NAME OF RESPONSIBLE PERSON K. Kim Luu
a. REPORT Unclassified	b. ABSTRACT Unclassified	c. THIS PAGE Unclassified			19b. TELEPHONE NUMBER (include area code) (808) 874-1608

20040607 044

OBJECT CHARACTERIZATION FROM SPECTRAL DATA

K. Kim Luu, Charles L. Matson, Capt Joshua Snodgrass
Air Force Research Lab, Directed Energy Directorate, 535 Lipoa Parkway, Suite 200, Kihei, HI 96753
S. Maile Giffin

Oceanit, 590 Lipoa Parkway, Suite 264, Kihei, HI 96753
Kris Hamada, John V. Lambert
Boeing LTS, 535 Lipoa Parkway, Suite 200, Kihei, HI 96753

**CLEARED
FOR PUBLIC RELEASE
AFRL/DEO-PA
2 SEP 03**

ABSTRACT

In general, the task of identifying the shape, function, and status of objects from nonimaging temporally-resolved spectral data is impossible. This is due to the limited degrees of freedom in the data as compared to the degrees of freedom that define shape, function, and status. However, by modeling objects as combinations of simple shapes with simple reflective and spectral characteristics, the problem though daunting is expected to become tractable due to the reduction of degrees of freedom in object space. One anticipated result from this modeling process is that the properties of null and near-null object features can be characterized; that is, an object can be characterized as a set of observable features summed with null or near-null features that perturb the measurement only slightly or not at all. The initial development of classes presented in this paper is a first step towards an inversion procedure to map spectral data into classes.

1. INTRODUCTION

Images of an orbiting satellite can be an excellent way to determine many of its important properties such as the functions that it can perform, its current status (operative or inoperative), and the mission in which it is engaged. For this reason, research has been carried out for many years to develop ways to obtain high resolution images of orbiting satellites from the ground. These years of research have culminated in a variety of adaptive optics systems and/or post-processing algorithms capable of producing images with spatial resolutions that are nearly diffraction-limited, depending upon the signal-to-noise levels in the measured data. However, there exists no reliable method to increase the spatial resolution in any image significantly beyond the limitations imposed by the telescope and observation wavelength combination. As a result, satellites in orbits beyond 1,000 km altitude generally cannot be imaged with high enough spatial resolution to be useful for determining function and status. In particular, geosynchronous satellites (in orbits at roughly 36,000 km) and the upcoming generations of micro-, nano-, and picosatellites are subject to this limitation with the current generation of ground-based optical telescopes.

Consequently, it is necessary to explore other means to interrogate satellites that cannot be imaged. One promising approach, discussed in this paper, is to collect data on these types of satellites that are resolved in dimensions other than spatial. For instance, spectrometers can be used to acquire wavelength-resolved information. If these spectral traces are obtained for multiple orientations of the satellite (i.e., at different times in a single pass for non-geosynchronous satellites or on different days for any satellite), the spectral traces will change depending upon the percentages of various material types illuminated by the Sun and visible from the ground site, thus adding a temporal dimension to the data. It is therefore reasonable to explore how simple geometric models might be developed to represent satellites that would reproduce the time-varying spectral traces. Because each of the basic shapes that make up the simple geometric models will in general have different spectral reflectances dependent upon their materials and paint, it appears feasible to determine the different materials composing each satellite. Such information can give insight into satellite function. As an example, the amount of power available to a satellite may be inferred from the size of the solar panels which can be inferred from the simple geometric model and analysis of the amount of blue in the spectral traces. It also might lead to plausible conclusions about satellite type based upon the simple geometric shape inferred from the time-varying spectral traces and from prior knowledge of the types of satellites currently in orbit.

Previous work in identifying satellites from their spectral signatures concentrated on determining if the spectral signatures alone were sufficient to group satellites into classes where each class consisted of similar satellites. For example, it has been discovered that, if a series of satellites existed that were made by the same manufacturer and had only minor differences between individual spacecraft, the spectral signatures were sufficiently similar to be able

DISTRIBUTION STATEMENT A
Approved for Public Release
Distribution Unlimited

A. EDI ME 23-420

OBJECT CHARACTERIZATION FROM SPECTRAL DATA

K. Kim Luu, Charles L. Matson, Capt Joshua Snodgrass

AMOS (Air Force Research Laboratory), 535 Lipoa Parkway, Suite 200, Kihei, HI 96753

S. Maile Giffin

AMOS (Oceanit), 590 Lipoa Parkway, Suite 264, Kihei, HI 96753

Kris Hamada, John V. Lambert

AMOS (Boeing LTS), 535 Lipoa Parkway, Suite 200, Kihei, HI 96753

ABSTRACT

In general, the task of identifying the shape, function, and status of objects from nonimaging temporally-resolved spectral data is impossible. This is due to the limited degrees of freedom in the data as compared to the degrees of freedom that define shape, function, and status. However, by modeling objects as combinations of simple shapes with simple reflective and spectral characteristics, the problem though daunting is expected to become tractable due to the reduction of degrees of freedom in object space. One anticipated result from this modeling process is that the properties of null and near-null object features can be characterized; that is, an object can be characterized as a set of observable features summed with null or near-null features that perturb the measurement only slightly or not at all. The initial development of classes presented in this paper is a first step towards an inversion procedure to map spectral data into classes.

1. INTRODUCTION

Images of an orbiting satellite can be an excellent way to determine many of its important properties such as the functions that it can perform, its current status (operative or inoperative), and the mission in which it is engaged. For this reason, research has been carried out for many years to develop ways to obtain high resolution images of orbiting satellites from the ground. These years of research have culminated in a variety of adaptive optics systems and/or post-processing algorithms capable of producing images with spatial resolutions that are nearly diffraction-limited, depending upon the signal-to-noise levels in the measured data. However, there exists no reliable method to increase the spatial resolution in any image significantly beyond the limitations imposed by the telescope and observation wavelength combination. As a result, satellites in orbits beyond 1,000 km altitude generally cannot be imaged with high enough spatial resolution to be useful for determining function and status. In particular, geosynchronous satellites (in orbits at roughly 36,000 km) and the upcoming generations of micro-, nano-, and picosatellites are subject to this limitation with the current generation of ground-based optical telescopes.

Consequently, it is necessary to explore other means to interrogate satellites that cannot be imaged. One promising approach, discussed in this paper, is to collect data on these types of satellites that are resolved in dimensions other than spatial. For instance, spectrometers can be used to acquire wavelength-resolved information. If these spectral traces are obtained for multiple orientations of the satellite (i.e., at different times in a single pass for non-geosynchronous satellites or on different days for any satellite), the spectral traces will change depending upon the percentages of various material types illuminated by the Sun and visible from the ground site, thus adding a temporal dimension to the data. It is therefore reasonable to explore how simple geometric models might be developed to represent satellites that would reproduce the time-varying spectral traces. Because each of the basic shapes that make up the simple geometric models will in general have different spectral reflectances dependent upon their materials and paint, it appears feasible to determine the different materials composing each satellite. Such information can give insight into satellite function. As an example, the amount of power available to a satellite may be inferred from the size of the solar panels which can be inferred from the simple geometric model and analysis of the amount of blue in the spectral traces. It also might lead to plausible conclusions about satellite type based upon the simple geometric shape inferred from the time-varying spectral traces and from prior knowledge of the types of satellites currently in orbit.

Previous work in identifying satellites from their spectral signatures concentrated on determining if the spectral signatures alone were sufficient to group satellites into classes where each class consisted of similar satellites. For example, it has been discovered that, if a series of satellites existed that were made by the same manufacturer and had only minor differences between individual spacecraft, the spectral signatures were sufficiently similar to be able

to identify the series of satellite model to which they belong. Much of the research in this area concentrated on identifying the optimal spectral bands for identification purposes and developing algorithms to classify the satellites into classes in a robust manner.

To much less of an extent, temporal variations in measured spectral signatures also have been used to determine object characteristics. The previous research in fact has primarily concentrated on using light curves (i.e., the spectral integral of the temporally-varying spectral signatures) to determine basic features of objects. For instance, light curves have been used to determine the shapes, rotation periods, pole direction, and scattering parameters of asteroids and artificial objects such as rocket bodies.

The goal of this research project is to integrate and extend previous results to build simple geometric and materials models of satellites from temporally-resolved spectral signatures. This extends previous research by adding the capability of building a satellite model, not just identify which satellites it is similar to, and obtain its overall dimensions. A primary objective supporting this goal is to characterize the spectral and spatial features on a satellite that can be determined from the temporally-varying spectral signatures and those that cannot be determined. In terms of the mathematical model describing the forward problem of how a satellite's spatial and spectral features produce the temporally-varying spectral traces, this objective can be stated as determining the null space of the forward operator. In general, of course, this objective is unachievable because the dimensionality of the data and the types of data result in null spaces that are far too large to obtain meaningful results for arbitrary objects. However, because the physical and spectral features of orbiting satellites are fairly distinct and limited, the domain of the forward problem may be small enough to permit meaningful results to be obtained. The second objective is to exploit the results from the first objective and develop algorithms that can be used to build the simple satellite models described earlier.

In this paper, current results are described. Meaningful progress has been made in developing forward models predicting the spectral and temporal signatures that would be measured for an orbiting satellite, though only the spectral work is presented here. A constrained weighted least squares algorithm has been implemented and exercised for estimating the fractional abundances of materials in the measured spectral traces based upon the spectral forward model. A key component of the spectral forward and inverse problems is determining the types of materials that generate spectral signatures sufficiently similar that they are best represented as realizations from a single material class, and those that are sufficiently dissimilar that they can be reliably estimated as belonging to separate material classes. These results are preliminary in that, although they demonstrate a good potential to identify the materials contributing to a spectral signature, there exist significant issues still to be resolved, such as local minima in the nonlinear algorithm cost function minimization, determination of appropriate classes for materials, and how to account for unmodeled or excess classes in the forward problem. Analysis to exploit the temporal variations in the spectral signatures to obtain shape information has also begun.

The paper is organized as follows: the mathematical model and associated issues in developing the spectral classes for the forward problem are described in Section 2; the properties of the simulated and real data used to test the validity of the forward problem are related in Section 3; the nonlinear inversion algorithm and results are discussed in Section 4; and conclusions and future work are given in Section 5.

2. THE FORWARD MODEL AND ASSOCIATED ISSUES

A large body of research exists in the areas of image analysis and object characterization using spectral and temporal signatures. For instance, multispectral and hyperspectral imaging sensors have been utilized for decades, especially with satellites imaging the Earth. These sensors obtain a series of images of the same scene but at different wavelengths, thus providing a spectral signature for each image pixel. These spectral traces can be used as input to *spectral unmixing algorithms* to estimate the materials that contribute to each pixel in the series of images. Such algorithms can use either linear or nonlinear models to describe the detected spectral signature resulting from the incident light interacting with the materials. In addition, either linear or nonlinear inversion algorithms can be used to invert the forward problem to determine the materials present in the measured spectral signature.

The current work builds upon these techniques to characterize spacecraft based upon temporally-varying spectral signatures captured in a single spatial pixel. A linear forward model may be assumed to apply in this problem since

spacecraft surface materials are arranged in discrete, segregated patches rather than mixed on spatial scales smaller than the path length of photons in the mixture, the situation in which nonlinear processes dominate [1]. As such, incident light is assumed to interact with just one component on the spacecraft prior to detection. Referring to the fractions in which materials appear in the mixed spectra as *fractional abundances*, the mixed spectra is thus modeled as a linear combination of each individual material spectra, called *endmembers*, weighted by its fractional abundance with the addition of a term to represent uncertainty in the model and sensor noise.

2.1 Mathematical Model

The linear forward model is represented explicitly by the following system:

$$\mathbf{x} = \mathbf{S}\mathbf{a} + \mathbf{w}$$

in which \mathbf{x} is a vector of time-resolved spectral measurements; \mathbf{S} is the system matrix mapping fractional abundances to mixed spectra; \mathbf{a} is a vector of time-resolved fractional abundances; and \mathbf{w} accounts for randomness in the measurement due to model uncertainty as well as sensor noise where it is assumed that the noise is independent pixel to pixel with covariance matrix \mathbf{W} . Of highest interest is the formulation of the system matrix consisting of basis functions, which must span the object space. Each spectral class is represented by a basis function, an appropriate form and quantity of which must be determined.

2.2 Spectral Classes

To form appropriate spectral classes, the surface materials of the typical satellites were identified. Six materials were selected to form unique classes: solar cell, white paint, aluminum, Mylar, red plastic, and yellow paint. The latter two materials are less common on spacecraft and are included primarily to examine the effects of including materials not present in the mixture on the inversion process. All materials were measured in a laboratory environment. Multiple spectral signatures for each of the first four materials were obtained while red plastic and yellow paint are characterized each by a single trace. However, the spectral traces for each material did not come from the same laboratory which posed difficulties as will be discussed later.

Thirty spectral traces of solar cell were obtained from a report issued by ERIM [2]. The original data set was not available so a line-tracing program developed in MATLAB was used to recreate the spectral trace from a scanned copy of the original document. An interpolation function provided intermediate wavelength points for higher resolution. Fig. 1 shows the thirty spectral traces for solar cell. The wavelength range is from 0.351 to 1.891 μm with 0.01 μm resolution and is plotted against reflectance. The peak is observed at approximately 0.39 μm , which is in the blue and very characteristic of solar cell material. A steep drop off occurs near 0.4 μm , and the curve flattens out after 0.5 μm . The samples are uniform around the peak reflectance and begin to exhibit more variations from 1 μm onwards.

Out of the 10 spectral traces for white paint, 6 of these were also sourced from the ERIM report. The same method used to generate data points for the solar cell traces was repeated. The remaining four traces were obtained from Jorgensen [3], which include glossy, flat, and chemglaze varieties of white paint. The steep rise occurring around 0.4 μm is very characteristic of white paint [3]. The spectrum is relatively flat over the visible wavelength range as expected and features a dip around 1.7 μm , consistently seen in all samples. The two spectral traces that appear quite different to the other eight are of flat white paint and glossy white. All other paints are of a chemglaze variety. The chemglaze paints seem to exhibit a double absorption feature (double dip) around 1.7 μm , not seen in the other two traces. The chemglaze paints also start a decrease in reflectivity around 0.5 μm , whereas the other two paints show a consistent reflectivity over a longer wavelength range. These differing characteristics might be a way of separating types of paints in the future, but for now all white paints are included in one class.

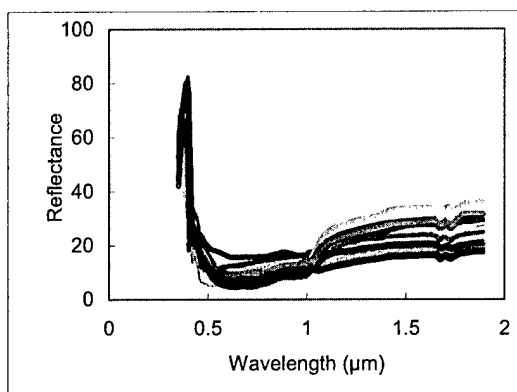


Fig. 1. Thirty solar cell spectral traces

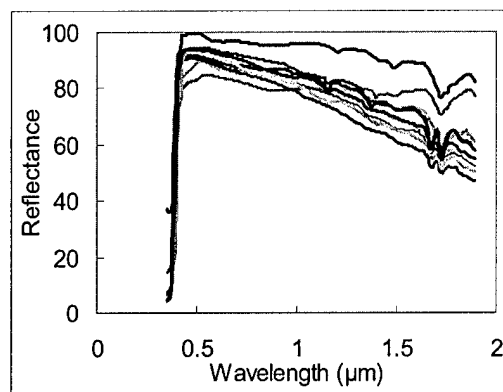


Fig. 2. Ten white paint spectral traces

The aluminum class contains eight traces. Four spectral traces were sourced from Jorgensen [3], three from the TASAT materials database [4], and one from the AFRL Satellite Assessment Center [5]. The eight materials are not of the same finish; various finishes were applied to several of the materials, including polished, mill, and cast aluminum. At this stage in the research all aluminum are included in one class because all materials exhibited spectral features inherent to aluminum. An absorption feature (dip in reflectivity) occurs around $0.85 \mu\text{m}$ and is consistently seen in all aluminum samples. Jorgensen [3] showed the strength of this inherent aluminum feature changed depending on the composition of the aluminum and furthermore states that this can be used to distinguish between types of aluminum, such as pure grade and high strength grade. As with the various white paints, future research will investigate if the different types of aluminum are distinguishable and whether they can be treated as separate classes.

The last class of materials to contain multiple spectral traces is Mylar. Laboratory spectral traces for this material were very difficult to find. Only three spectral traces for Mylar were found in the Satellite Assessment Center materials database [5]. Using these traces, nine more were produced by random composites of the original three. Fig. 4 shows twelve spectral traces for Mylar. The reflectance for Mylar is very flat over a broad wavelength range and only one out of the three original traces included an absorption feature at $1.6 \mu\text{m}$.

Since the spectral traces come from various sources, it is necessary to normalize the traces to reduce the measurement offset inherent in different spectrometers. For simplicity, it was assumed that if a similar amount of energy is received from all like samples, then the most appropriate method for normalizing the aluminum traces is by the area under the curve. The reflectance values are then rescaled to match the other three materials.

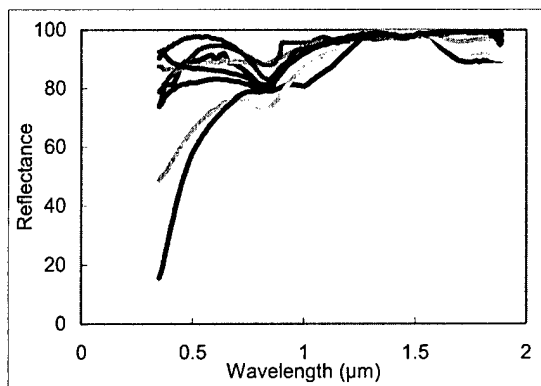


Fig. 3. Eight aluminum spectral traces

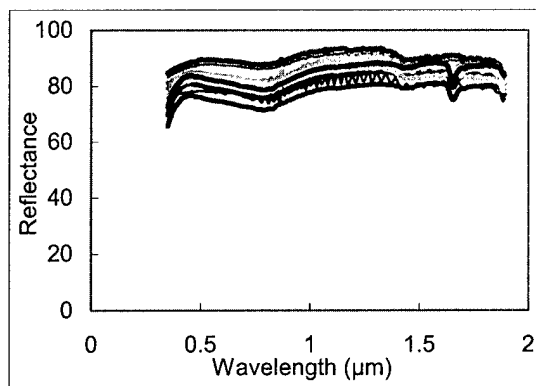


Fig. 4. Twelve Mylar spectral traces

2.3 Class Representation

The system matrix contains the spectral basis functions for each of the six classes. If the object space is spanned, then some unique combination of the spectral basis functions should produce the measured spectrum obtained from an observation. The spectral basis function for classes with multiple traces is taken as the mean of each wavelength bin so that in essence, the average of multiple spectral traces of the same material forms the basis function. For red plastic and yellow paint, the single trace for each class also serves as its basis function.

The mean spectral traces for each class with one standard deviation are shown in Fig. 5-9. Due to the similarity of spectral traces within the solar cell and white paint classes, the mean follows closely the shape of any one of the individual traces. However for aluminum, the standard deviation is very high at the blue end of the spectrum where most of the variation occurs in the samples. The variance for the aluminum class is larger than the other materials. This is obvious by inspection of Fig. 3 and is also consistent with the fact that a wide variety of aluminum samples composes the class. This may be a possible source for problems in the inversion process. The Mylar class shows a small standard deviation due to the simulated traces being composites of the three original laboratory measurements.

As mentioned earlier, within a single class, materials have a certain amount of variability between them. The magnitude of this variability is captured in the statistical variance as a function of wavelength for each class. The variance, scaled by the corresponding fractional abundance of that class, determines the class size for each material which in turn represents model uncertainty. Since fractional abundance is time-resolved, the model uncertainty is also a function of time as well as wavelength.

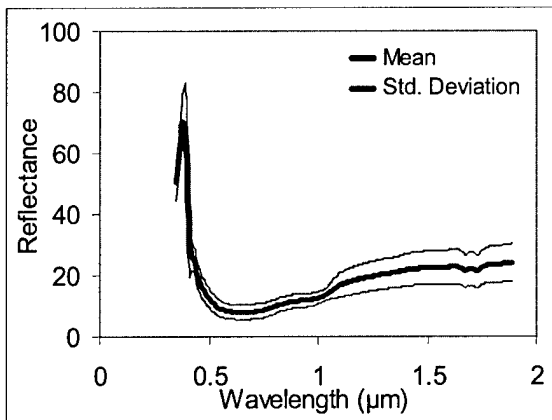


Fig. 5. Basis function and size of solar cell class

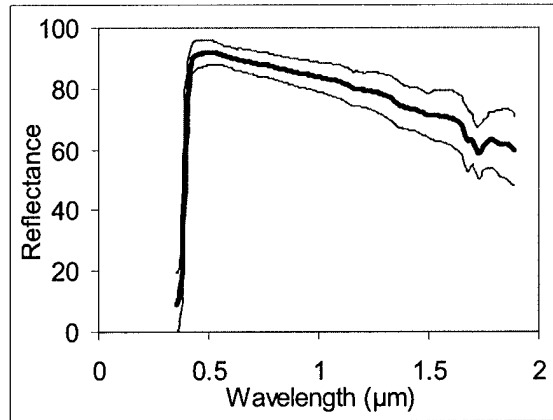


Fig. 6. Basis function and size of white paint class

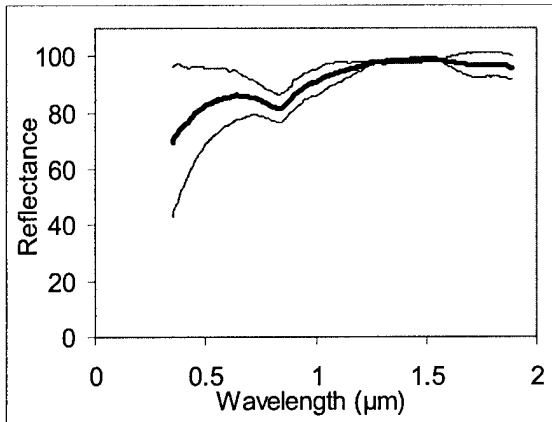


Fig. 7. Basis function and size of aluminum class

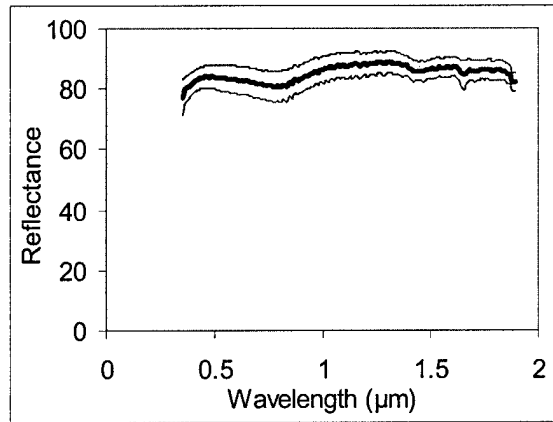


Fig. 8. Basis function and size of Mylar class

3. REAL AND SIMULATED SPECTRAL OBSERVATIONS

As a means of evaluating the performance of theoretical nonimaging SOI techniques, observational data from the Spica Spectrometer was considered. The Spica sensor is an AFRL instrument located on the rear blanchard of the 1.6m telescope at the AMOS facility on Haleakala, Maui, shown in Fig. 9. The central component of the sensor is a commercially available spectrometer produced by Acton Research with a 150 lines per millimeter grating that yields a 0.3 to 0.4 nm resolution. It is equipped with a liquid nitrogen cooled, 1100 by 330 pixel Princeton Instruments CCD which provides a sensitivity limit of 14th magnitude objects. In its current configuration, Spica can provide photometric and spectroscopic data in two wavelength coverage modes. The blue mode provides spectra from 0.4 to 0.7 μm and a red mode provides data in the 0.6 to 0.9 μm regime [6]. Spica is a dedicated non-imaging SOI spectrometer that has collected data in support of several projects whose purposes have ranged from materials detection and space-environment effects to theoretical and neural network classification schemes [7-9].

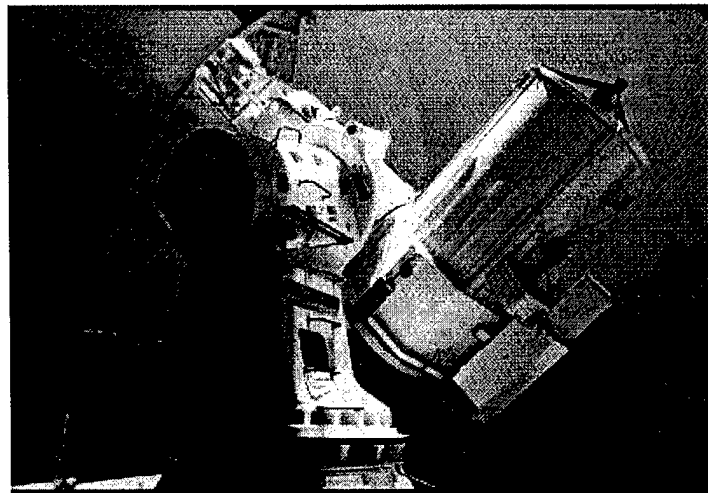


Fig. 9. The Spica spectrometer on the 1.6m telescope

3.1 Data Calibration

Standard astronomical techniques are used in the calibration of spectral data for wavelength location, atmospheric extinction, and instrumental sensitivity. Wavelength calibration on the spectra is provided through the use of calibration lamps, a Mercury lamp for blue-mode spectra, and an Argon lamp for red-mode spectra. In order to remove the color-altering effects of scattering and CCD sensitivity, a widely accepted astronomical data reduction software package, the Image Reduction and Analysis Facility (IRAF) developed at the Kitt Peak National Observatory, is used. These procedures utilize data from a set of catalogued spectral standard stars in order to generate an instrument and seeing-condition specific sensitivity function that is then applied to object data to produce calibrated intensity data. With wavelength, intensity, and atmospheric calibrations accomplished, the spectra are calibrated, exo-atmospheric, spectral data. Because satellite spectra are reflected solar light, solar features must next be removed to reveal material features of the object. To do this, the exo-atmospheric spectra are divided by solar-class stars collected through Spica and calibrated in the same manner as the object data.

3.2 Observations

As a test case for this project, it was desirable to use data of an object that had a relatively simple structure and yet possessed the possibility of photometric variation under some illumination and observation conditions. Based upon these criteria, cylindrical objects were selected as evaluation cases; in particular, the Boeing 376 class of communication satellites was chosen. This satellite class is composed of a cylindrical, spun body wrapped with solar panel. It contains a telescoping section that extends upon deployment and a band of reflective material on the upper portion with a de-spun Mylar-covered antenna at one end of the cylinder. An illustration of the Boeing 376 bus is shown in Fig. 10. Boeing 376 satellites are positioned in a north-south alignment typically at geo-

synchronous orbits. This makes the class an attractive target because of the stability of the illumination and observation conditions. A particular set of observations (Fig. 10 and 11) was taken in March 2003 on Galaxy V, a member of this class, at various times throughout a full night of observations. Under these observing conditions the phase angle, or the angle from the Sun to the satellite to the observer, varies over a large range. This particular data set shows that the color of the object remains stable aside from a few cosmic rays. In addition, a large blue component to the spectra indicates the presence of a reflection from the solar panel material wrapped around the cylindrical body.

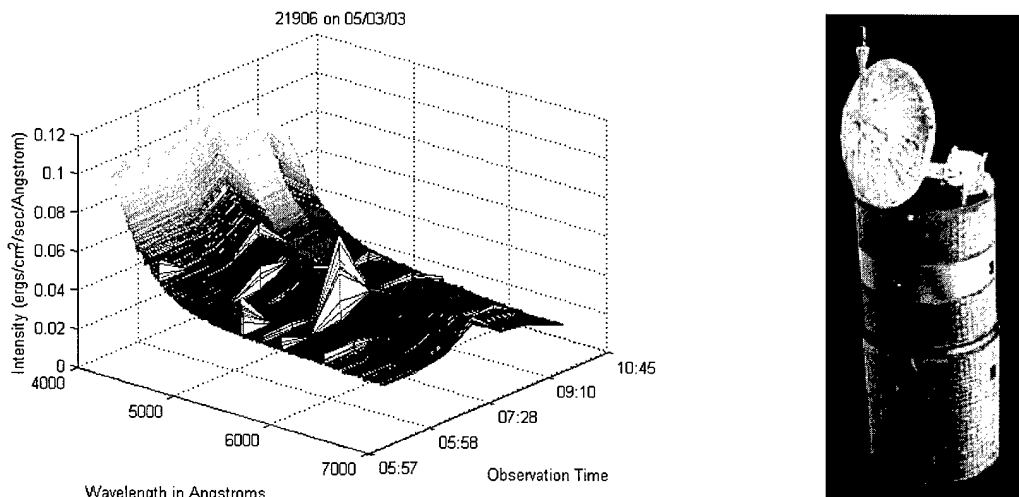


Fig. 10. At left, a surface plot of the spectra collected. At right, a depiction of a typical Boeing 376 satellite.

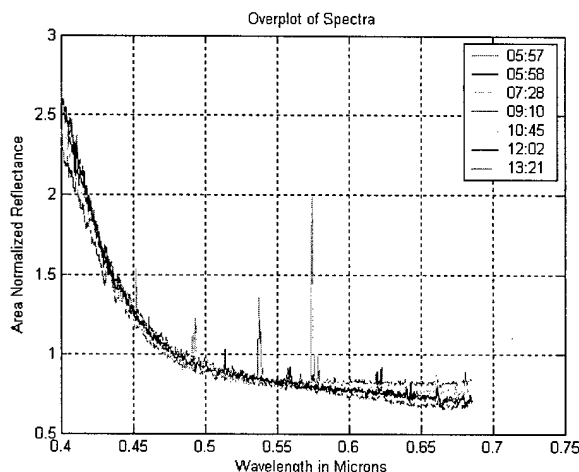


Fig. 11. The spectra collected are shown overlaid. Observation times in UT are shown in the legend.

3.3 Simulated Observations

In an effort to aid the analysis of the Galaxy V, simulations of a Boeing 376 satellite were performed in TASAT. The satellite model was generated in the Satellite Modeling Tool software and was composed of a large solar panel wrapped cylinder and a smaller solar panel wrapped cylinder with a band of aluminum inserted for the reflective strip. The model was then set to fly the orbit of Galaxy V at the time of the Spica observations. The passive cross-section of each separate component and the object as a whole were produced as the end product from TASAT. Typical ground-measured material spectra for aluminum and solar panel were selected and applied to the appropriate component passive cross-section, and integrated whole spectra were produced for each observation in the Spica data

set. The results of the simulation are shown in Fig. 12 and 13. In the TASAT generated image, the aluminum strip is multi-colored showing that it is the brightest component in this particular image. Darker shades of blue correspond to lower intensities. The simulation results are reasonable when compared with the observations and show that the stability of the spectra for this particular object is explained by its symmetry with respect to the phase angle variation. In addition, the simulated data provided a noise-free test set that ranged from 0.351 to 1.891 μm with which to test the inversion algorithm. Most importantly, the expected contribution of specific material classes is known.

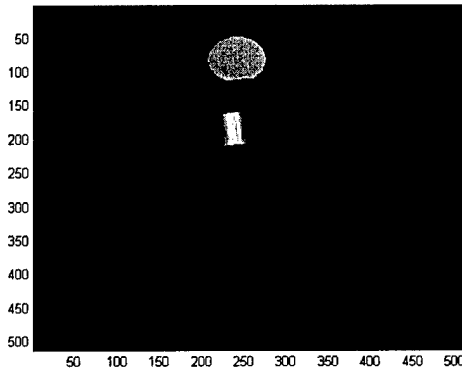


Fig. 12. TASAT generated image in false color

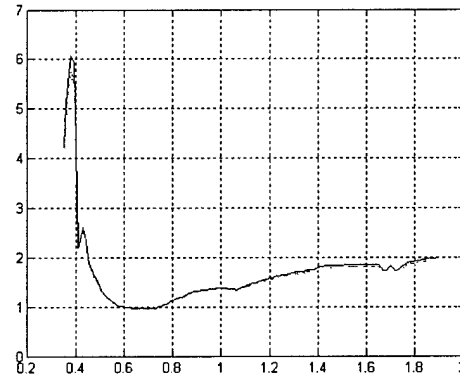


Fig. 13. Simulated spectra

4. IMPLEMENTATION OF THE INVERSION ALGORITHM AND RESULTS

Spectral unmixing involves two separate issues. First, the endmembers present in the mixed spectra must be determined. This enables the second step, estimating the fractional abundances of the material classes or *inversion*. A constrained weighted least squares approach is taken for inversion while endmember determination has not been addressed in the current work. The importance of examining the first issue in future efforts is stressed by noting that inversion with endmembers not actually present in the mixed spectra may lead to erroneous results since least squares will indiscriminately minimize fitting errors with any endmembers made available to the algorithm [1]. The results in this paper assume that the appropriate classes are known in advance of applying the inversion algorithm.

4.1 Mathematical Model

The cost associated with the inverse model is

$$J(\mathbf{a}) = (\mathbf{x} - \mathbf{S}\mathbf{a})^T \mathbf{W}(\mathbf{x} - \mathbf{S}\mathbf{a}) + \lambda_1 \left\| \sum a_i - 1 \right\|^2 + \lambda_2 \left\| \partial \mathbf{a} / \partial t \right\|^2$$

The first term of the cost function deals with fitting the observational data to the system model. While both model uncertainty and sensor noise may be included in the covariance matrix \mathbf{W} , no sensor noise is currently modeled since preliminary estimations indicate that model uncertainty is overwhelmingly larger than anticipated sensor noise. The remaining terms are constraints to the estimation problem weighted by Lagrangian multipliers. The first constraint enforces full additivity, which is the notion that the fractional abundances should add up to one at each estimation time. The other constraint ensures temporal smoothness, arising from the reasoning that fractional abundances would vary smoothly from one observation to the next of a single spacecraft. To ensure that fractional abundances are nonnegative, the square root of the fractional abundances is actually estimated. The inclusion of the full additivity constraint and the nonnegativity constraint makes the inversion algorithm nonlinear.

This inversion algorithm is implemented in MATLAB using a conjugate gradient method for minimization. The optimization routine is adapted from the *fprmn* code in Numerical Recipes [10] and employs first derivative calculations and one-dimensional subminimization. The temporal information extraction for object shape and orientation is carried out separately, using the estimated material fractional abundances. This temporally-resolved

data contains information embedded from a range of illumination and viewing geometries for the spacecraft captured in the observations.

4.2 Simulated Data Results

Inversion results using the simulated observations for Galaxy V, discussed previously, are quite good (Table 1). In this case, the mixed spectra is generated with one particular trace each from the solar cell and aluminum classes while the inversion code works with the system matrix containing basis functions for the same classes. Estimated fractional abundances vary slightly with different initial guesses; the results reported in Table 1 are the average of nine trials with uniformly varying initial guesses. Percent differences from the truth are small, ranging from 0.05–4.2%. The temporal variation is well tracked except for a deviation at Observation 5. Most importantly, these solid results demonstrate the validity of the forward model.

Table 1. Inversion Results for Simulated Galaxy V Data

Observation	1	2	3	4	5	6	7
Truth							
Solar Cell	0.7075	0.7071	0.7004	0.6963	0.6957	0.7037	0.7370
Aluminum	0.2925	0.2929	0.2996	0.3037	0.3043	0.2963	0.2630
Inversion							
Solar Cell	0.7165	0.7165	0.7116	0.7083	0.7097	0.7180	0.7366
Aluminum	0.2852	0.2852	0.2901	0.2934	0.2920	0.2838	0.2651

4.3 Real Data Results

Using the actual observations for Galaxy V in the blue mode, which limits the wavelength range to 0.411–0.681 μm , the inversion results are more interesting. The endmembers included in the inversion are solar cell, aluminum, and Mylar, and results are shown in Fig. 14–16. Ten trials with varying initial guesses are plotted as well as the average. A numerical issue with local minima is apparent; nonetheless, averaging the results may still provide a good estimate of the global minimum. Estimates for the solar cell class, modeling the solar panels of the spacecraft, are slightly less than 60% for surfaces facing the sensor. From a priori knowledge of the spacecraft configuration and motion, this result is reasonable. The aluminum class is used here to hopefully represent the band of reflective material on the upper portion of the cylindrical body while the Mylar class covers the antenna. The estimates for these classes are about 20% each which again seems likely.

Also examined is data for Galaxy V in the red mode. Recall that the aluminum class features a characteristic dip near 0.85 μm which falls outside of the wavelength range covered by the blue mode. Data in the red mode ranges from 0.581 to 0.891 μm so possibly the inversion code may key on this feature. The estimates, reported in Fig. 17–19, differ significantly from the blue mode results. Contrary to expectations, the aluminum class (along with Mylar) has only a trace appearance. However, the red data is visually noisier than the blue data so preprocessing for spectral smoothness may change the results.

4.4 Modeling and Numerical Issues

These results raise several issues to be addressed in future work. It is apparent that local minima abound in the parameter space, and the solution is also very sensitive to the weighting by Lagrangian multipliers. Remedies to explore include genetic algorithms to select the best initial guesses and alternate optimization schemes. There is much previous work in this area for related problems to exploit. Of higher interest are the issues relating to the representation of the spectral classes. Specifically, the relationship between variance and separate classes should be addressed. For instance, it may be appropriate to split up the aluminum class by the various finishes, which impart significant differences in the spectral signatures. On the other hand, the set of basis functions must be linearly independent in order to ensure a unique solution by the inversion algorithm. Principal component analysis may be an important step to defining classes.

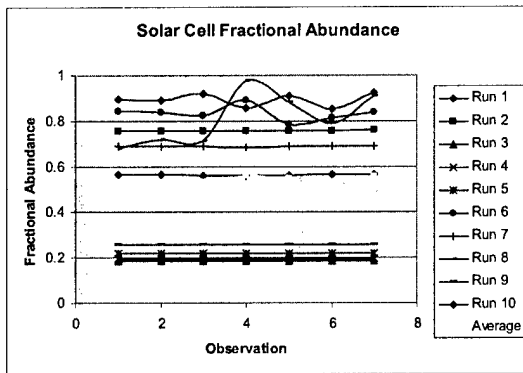


Fig. 14. Results of Blue Data for Solar Cell

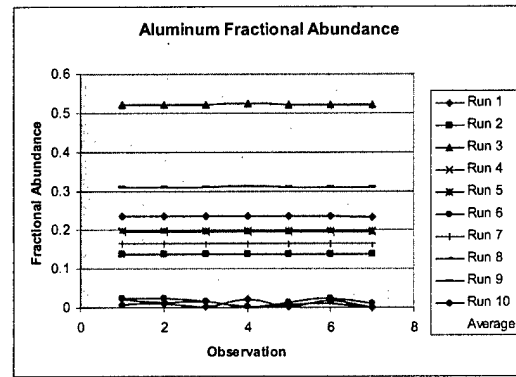


Fig. 15. Results of Blue Data for Aluminum

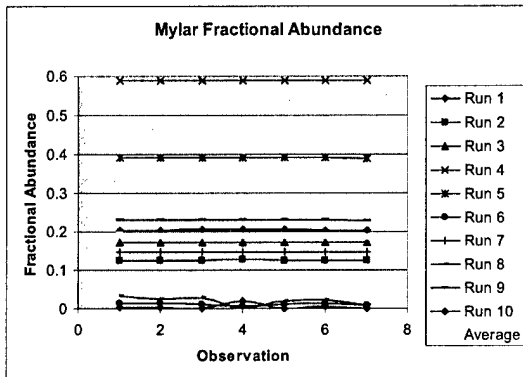


Fig. 16. Results of Blue Data for Mylar

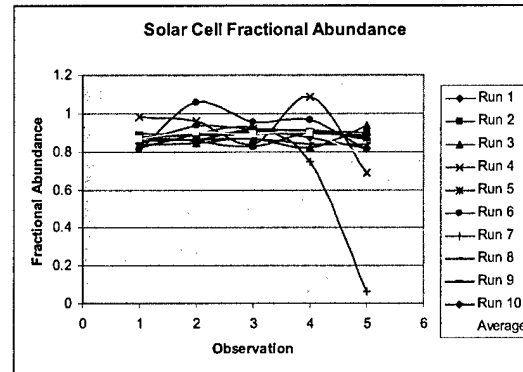


Fig. 17. Results of Red Data for Solar Cell

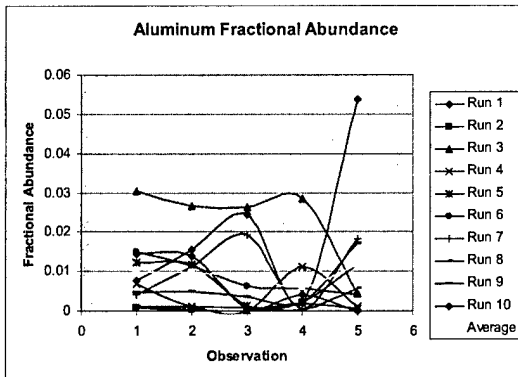


Fig. 18. Results of Red Data for Aluminum

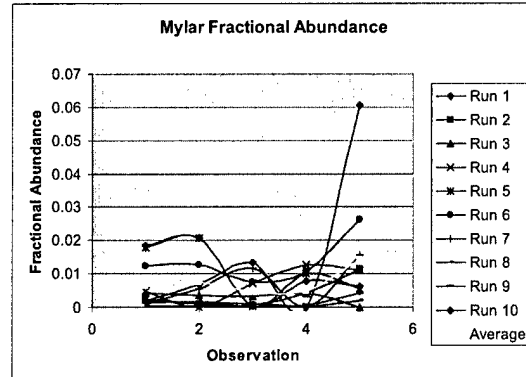


Fig. 19. Results of Red Data for Mylar

5. CONCLUSIONS AND FUTURE WORK

This work demonstrates that it is possible to identify classes of materials that underlie the measured spectral data from orbiting satellites. The results are quite preliminary and need further refinement to analyze problems associated with local minima in estimating the global minimum of a cost function used in the inversion algorithm. However, the results already point to underlying class identification and representation issues such as how to determine appropriate class sizes, how to generate useful representative traces for the classes, and how to deal with unmodeled and non-existent classes. As such, the algorithm assists in identifying how best to model the forward problem in order to determine what are the null material features of a satellite (i.e., the material features that cannot be separately/uniquely determined from the spectral data).

Future work includes exploiting the temporal dependences of the spectral data to obtain basic shape information of satellites. The mathematical models have been developed to describe the temporal variations in spectral signatures for a variety of basic shapes (cylinder, cube, etc.). Still to be accomplished is the development of methods to identify these basic shapes from temporal variations. An outflow of the temporal work will be insight into the null spatial features of an object. Additional future work includes a more rigorous analysis of the development of spectral classes for various material types and how to best represent the material types in the forward problem. The project will also explore other algorithms that may be more optimal in determining spectral classes from the measured data to ensure that conclusions are not a function of a specific algorithm used in the inversion process.

6. ACKNOWLEDGMENTS

This work was sponsored by the Air Force Office of Scientific Research, Directorate of Mathematics and Space Sciences. The authors gratefully acknowledge Dr. Clifford Rhoades and Maj. William Hilbun for their enthusiastic support.

7. REFERENCES

1. Keshava, N., and Mustard, J.F., Spectral Unmixing, *IEEE Signal Processing Magazine*, pp. 44-57, Jan 2002.
2. Bair, M.E., et al., Determination of Satellite Observables Vol. IV Optical Properties of Satellite Materials, Technical Report SAMSO TR-73-291 Vol. IV, May 1974.
3. Jorgensen, K.M., *Using Reflectance Spectroscopy to Determine Material Type of Orbital Debris*, Doctoral Thesis, University of Colorado, May 2000.
4. TASAT, Logicon Technology Solutions, Albuquerque, NM, May 2001.
5. Munson, P., Materials Database Version 5.0, Satellite Assessment Center, Air Force Research Laboratory, Nov 2000.
6. Nishimoto, D.L., et al., Spectroscopic Observations of Space Objects and Phenomena using Spica and Kala at AMOS, *Proceedings of SPIE*, Vol. 4490B, San Diego, CA, 29 Jul – 3 Aug 2001.
7. Jorgensen, K.M., et al., Determining the Material Type of Man-Made Orbiting Objects using Low-Resolution Reflectance Spectroscopy, *Proceedings of SPIE*, Vol. 4490B, San Diego, CA, 29 Jul – 3 Aug 2001.
8. Jorgensen, K.M. et al., Squiggly Lines and Why They are Important to You, 2002 Lincoln Space Control Conference, Lexington, MA, Mar 2002.
9. Jorgensen, K.M. et al., Using AMOS Telescope for Low Resolution Spectroscopy to Determine the Material Type of LEP and GEO Objects, *Proceedings of AMOS Technical Conference*, Wailea, HI, 10-14 Sep 2001.
10. W.H. Press et al., Numerical Recipes in FORTRAN: The Art of Scientific Computing, Cambridge University Press, 1994.